

Supplementary Information

Graphitic carbon nitride ornate with FeNi₃ nanoparticles for flexible planar micro supercapacitor with ultrahigh energy density and quantum storage capacity

Meenakshi Talukdar, Sushant Kumar Behera and Pritam Deb*

Advanced Functional Material Laboratory (AFML), Department of Physics, Tezpur University (Central University), Tezpur-784028, India.

*Corresponding author

Email address: pdeb@tezu.ernet.in (Pritam Deb)

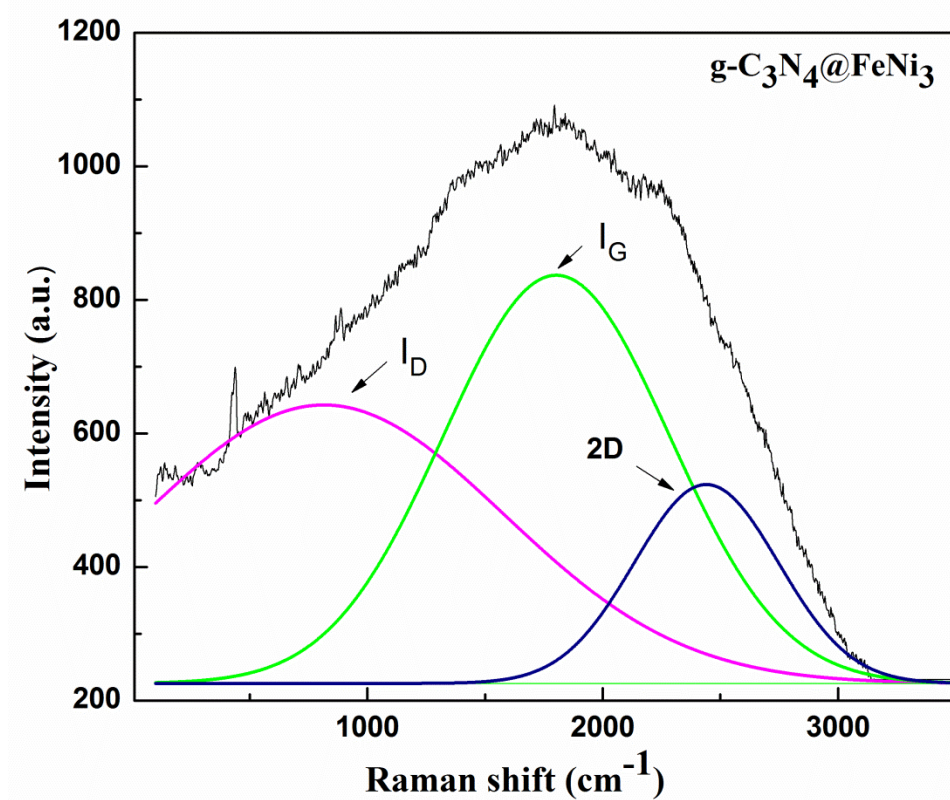


Figure S1: Raman curve for hybrid $g\text{-C}_3\text{N}_4@\text{FeNi}_3$ heterostructure

1. B. Wang, X. L. Li, B. Luo, J. X. Yang, X. J. Wang, Q. Song, S. Y. Chen, L. J. Zhi, *Small* 2013, **9**, 2399–2404.
2. X. Xu, C. Shi, Q. Li, R. Chen, T. Chen, *RSC Adv.* 2017, **7**, 14382.

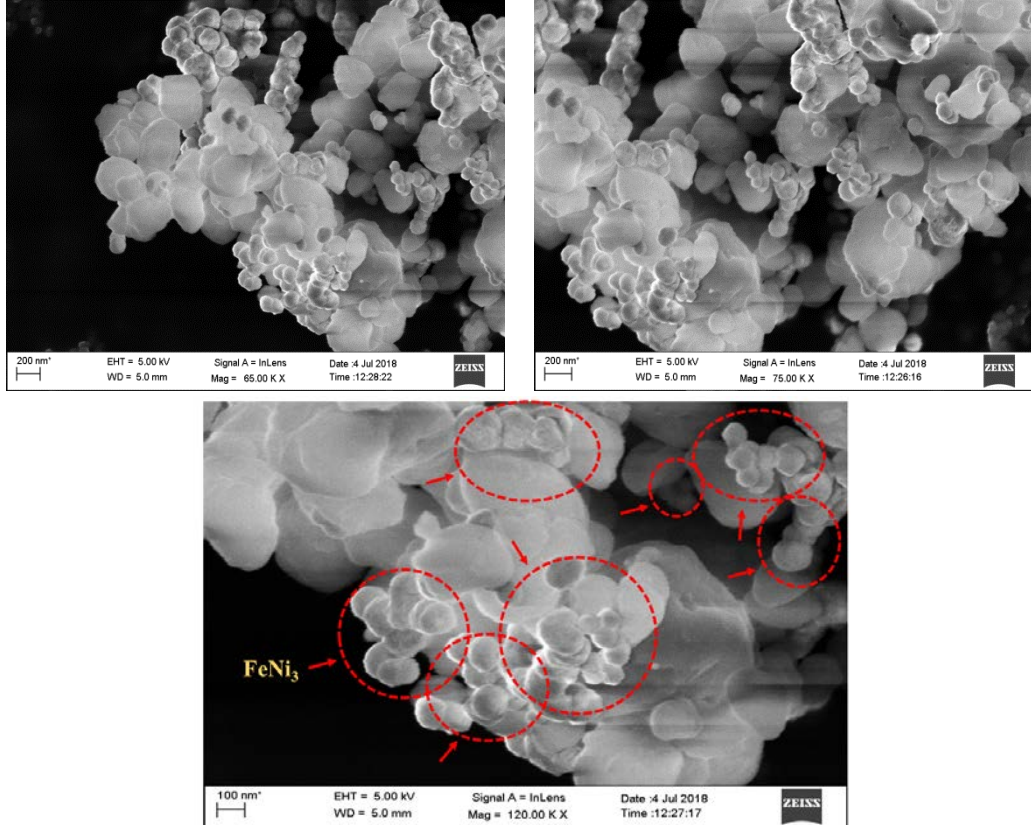


Figure S2: FESEM images of $\text{g-C}_3\text{N}_4@\text{FeNi}_3$ heterostructure at 200 nm magnification. Low magnification (100 nm) FESEM images of the same system. Red dotted circles are marked to show FeNi_3 clusters.

Material Name	Areal Capacitance (F/cm ⁻²)	Year	Reference No.
g-C ₃ N ₄ @FeNi ₃	19.21 mFcm⁻²		This work
CNT (Carbon Nano Tube)	0.428 mF cm ⁻²	2009	1
VS ₂ ultrathin nanosheets	4760 μ Fcm ⁻²	2011	2
VS2	4.7 mF cm ⁻²	2011	3
RuOx	12.6 mF cm ⁻²	2013	4
Phosphorene and Graphene	9.8 mFcm ⁻²	2017	5
rGO/TiO ₂ NR/rGO	13.74 mF cm ⁻²	2013	6
CNT (Carbon Nano Tube)	1.9 mF cm ⁻²	2015	7
Graphene base RMGO	394 μ Fcm ⁻²	2011	8
Graphene base RGO	462 μ Fcm ⁻²	2013	9
Graphene-based in-plane micro-supercapacitors	80.7 μ Fcm ⁻²	2013	10
C-onion (carbon onion)	0.9 mF cm ⁻²	2010	11
PyP (pyrolyzed photoresist)	0.6 mF cm ⁻²	2014	12
Activated carbon	2.1 mF cm ⁻²	2010	13
LSG, laser scribed graphene	5 mF cm ⁻²	2012	14
EG (Exfoliated Graphene)	5.4 mF cm ⁻²	2016	15
Graphene quantum dots	0.535 mF cm ⁻²	2013	16

Table S1: Comparative study table of g-C₃N₄@FeNi₃ heterostructure with other materials

References given for comparison

❖ This work...

1. Y.-Q. Jiang, Q. Zhou, L. Lin, Planar MEMS supercapacitor using carbon nanotube forests IEEE 22nd Int. Conf. Micro Electro Mechanical Systems (Sorrento, Italy, 25-29 January 2009) pp 587-90. **2009**.
2. J. Feng, X. Sun, C. Wu, L. Peng, C. Lin, S. Hu, J. Yang, Y. Xie, *J Am Chem Soc.* **2011**, 133(44),17832-8.
3. W. Gao, N. Singh, L. Song, Z. Liu, A.L. Reddy, L. Ci, R. Vajtai, Q. Zhang, B. Wei, P.M. Ajayan, *Nat Nanotechnol.* **2011**, 6(8),496-500.
4. Z. Niu, L. Zhang, L. Liu, B. Zhu, H. Dong, X. Chen, *Adv Mater.* **2013**, 25 (29), 4035-42.
5. H. Xiao, Z.S. Wu, L. Chen, F. Zhou, S. Zheng, W.Ren, H. M.Cheng, X. Bao, *ACS Nano.* **2017**,11(7),7284-7292.
6. Ramadoss, G.-S. Kim, S.-J. Kim, *CrystEngComm* **2013**, 15, 10222-10229.
7. D. Membreño, L. Smith, K.S. Shin, C.O. Chui, B. Dunn, *Transl. Mater. Res.* **2015**, 2 015001.
8. J.-J. Yoo, K. Balakrishnan, J. Huang, V. Meunier, B. G. Sumpter, A. Srivastava,M. Conway, A.-L.-M. Reddy, J. Yu, R. Vajtai, P.-M. Ajayan, *Nano Lett.* **2011**, 11, 1423-1427.
9. Z.-S. Wu, K. Parvez, X. Feng, K. Müllen, *Nat Commun.* **2013**,4, 2487.
10. S. Makino, Y. Yamauchi, W. Sugimoto, *J. Power Source* **2013**, 227, 153.
11. D. Pech, M. Brunet, H. Durou, P. Huang, V. Mochalin, Y. Gogotsi, P.L. Taberna, P. Simon, *Nat. Nanotechnol.* **2010**, 5, 651-4.
12. S. Wang, B. Hsia, C. Carraro,R. Maboudian, *J. Mater. Chem. A.* **2014**, 2, 7997.
13. D. Pech, M. Brunet, P.L. Taberna, P. Simon, N. Fabre, F. Mesnilgrente, V. Conédéra, H. Durou , *J. Power Sources* **2010**, 195, 1266-9.
14. E.K. M F, V. Strong, S. Dubin, B.R. Kaner, *Science* **2012**,335 1326-30.
15. L. Zhaoyang, Z.S. Wu, S. Yang, R. Dong, X. Feng, K. Müllen, *Adv.Mater.* **2016**, 28, 2217–2222.
16. W. W. Liu, Y. Q. Feng, X.-B. Yan, J.T. Chen, Q.J. Xue, *Adv. Funct. Mater.* **2013**, 23, 4111.

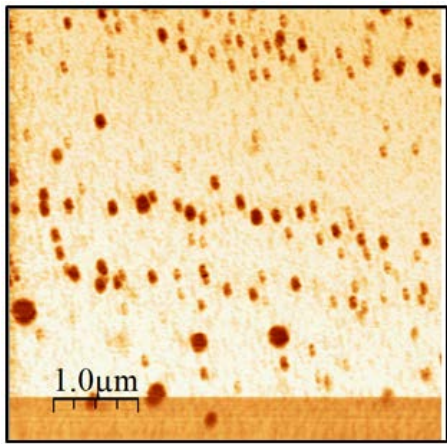


Figure S3: AFM image of $\text{g-C}_3\text{N}_4@\text{FeNi}_3$ heterostructure

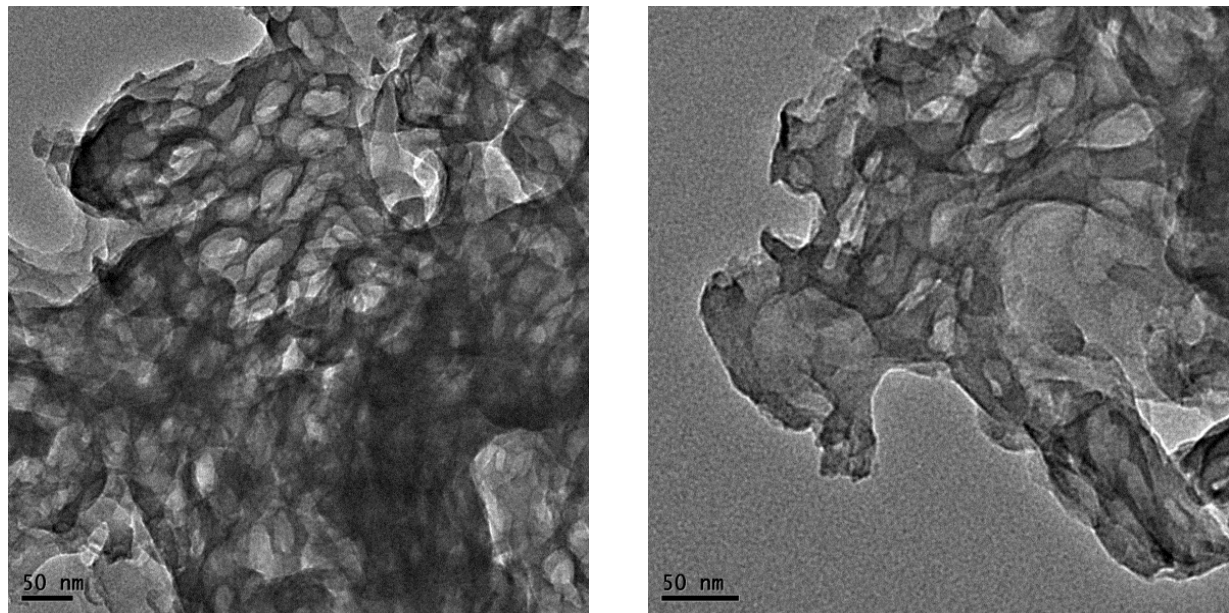


Figure S4: TEM images of graphitic carbon nitride

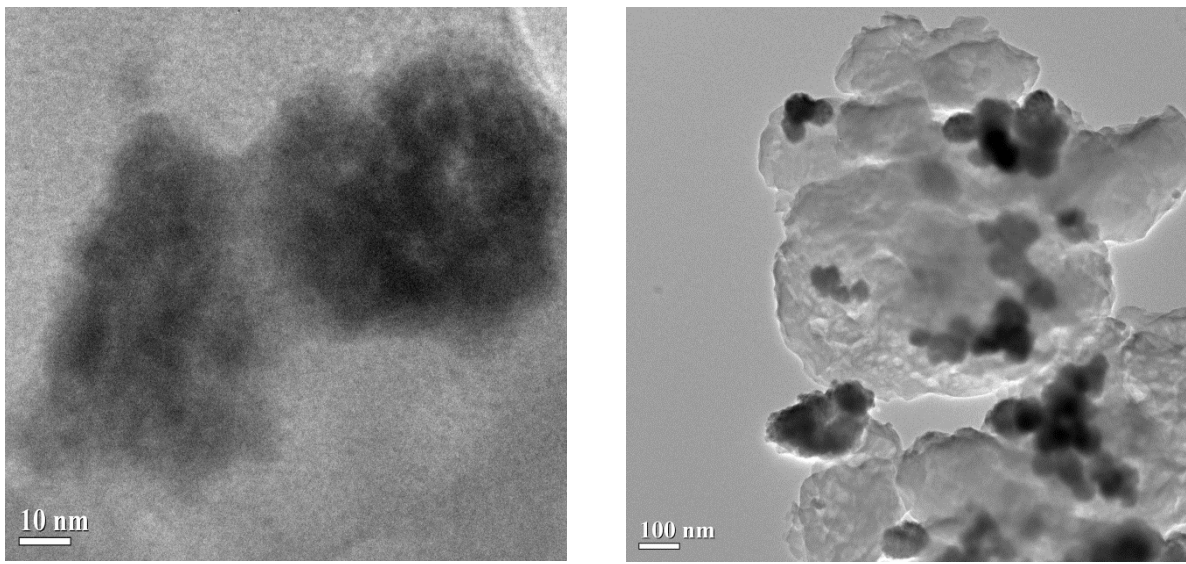


Figure S5: TEM images of g-C₃N₄@FeNi₃ heterostructure

Electronic structure showing the active edge states

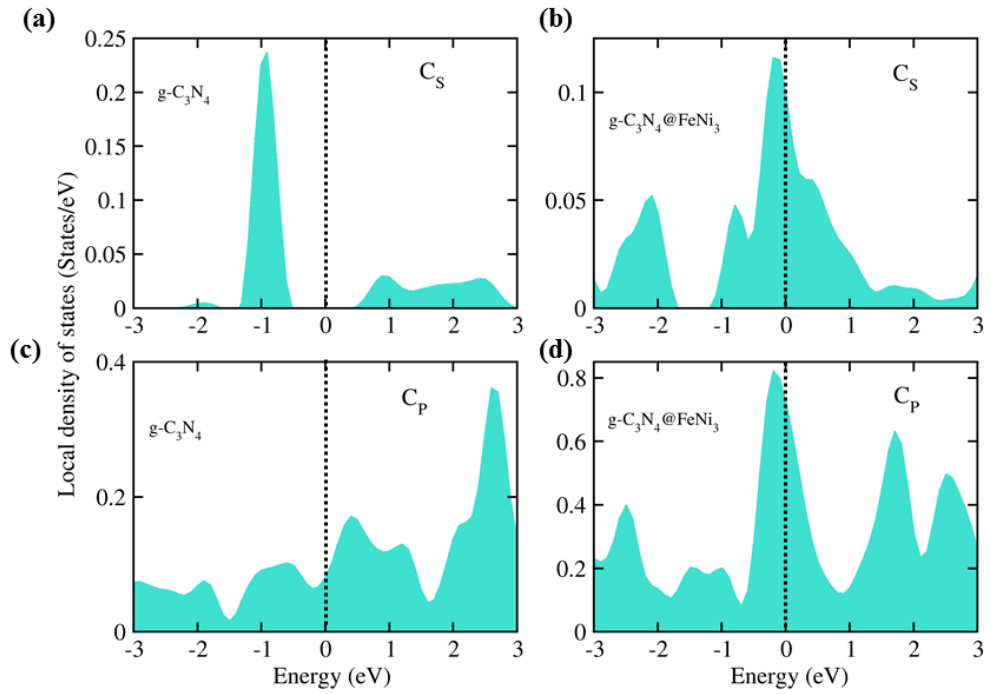


Figure S6. Local density of states of carbon s orbitals for (a) pristine $\text{g-C}_3\text{N}_4$ and (b) hybrid composite $\text{g-C}_3\text{N}_4@\text{FeNi}_3$. Similarly, the p orbital of carbon atom is shown in pristine $\text{g-C}_3\text{N}_4$ and (b) hybrid composite $\text{g-C}_3\text{N}_4@\text{FeNi}_3$. Black dotted line is showing the Fermi energy level.

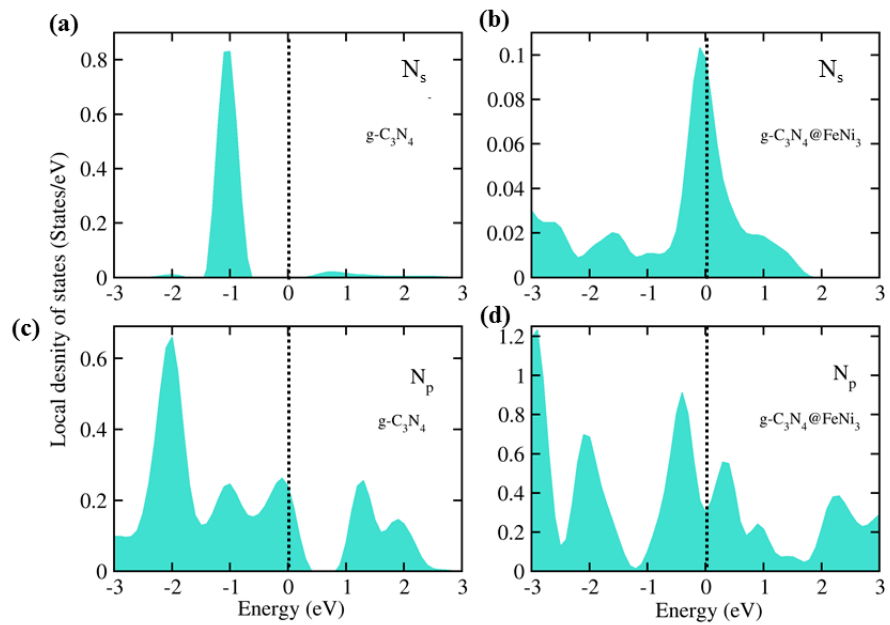


Figure S7. Local density of states of nitrogen s orbitals for (a) pristine $\text{g-C}_3\text{N}_4$ and (b) hybrid composite $\text{g-C}_3\text{N}_4@\text{FeNi}_3$. Similarly, the p orbital of nitrogen atom is shown in pristine $\text{g-C}_3\text{N}_4$ and (b) hybrid composite $\text{g-C}_3\text{N}_4@\text{FeNi}_3$. Black dotted line is showing the Fermi energy level.

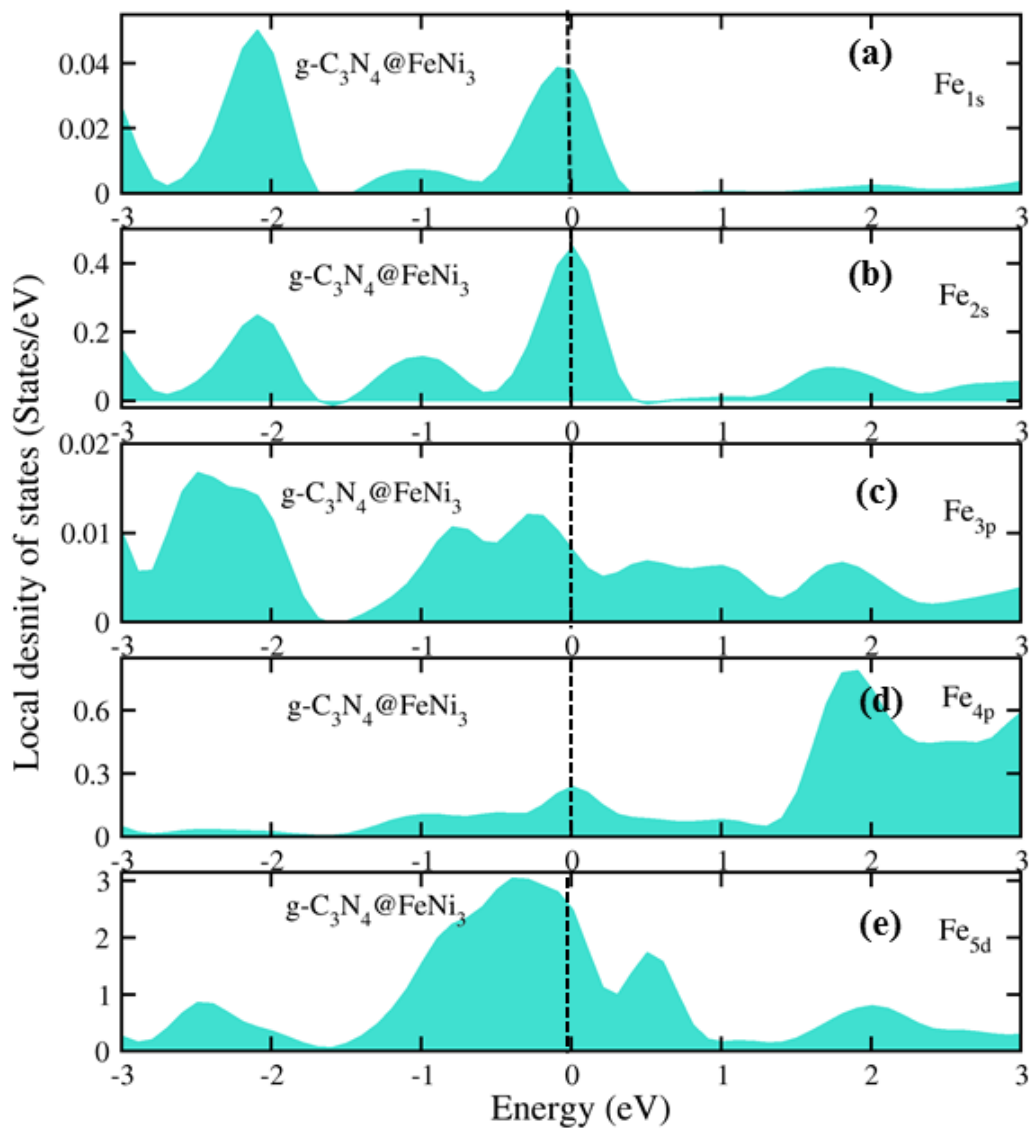


Figure S8. Local density of states of various orbitals in iron atom of the hybrid composite (a) 1s, (b) 2s, (c) 3p, (d) 4p and (e) 5d. Black dotted line is showing the Fermi energy level.

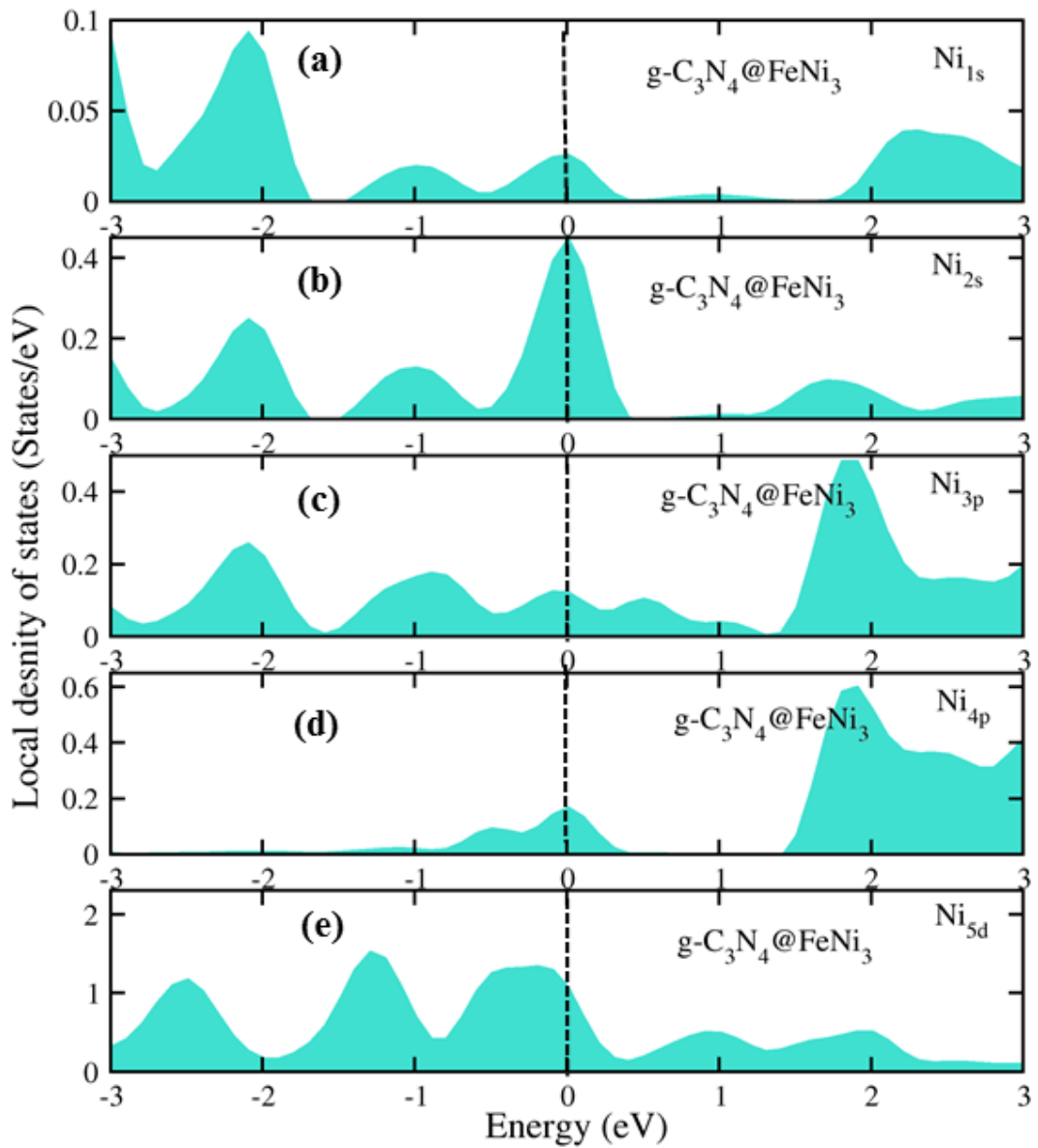


Figure S9. Local density of states of various orbitals in nickel atom of the hybrid composite (a) 1s, (b) 2s, (c) 3p, (d) 4p and (e) 5d. Black dotted line is showing the Fermi energy level.

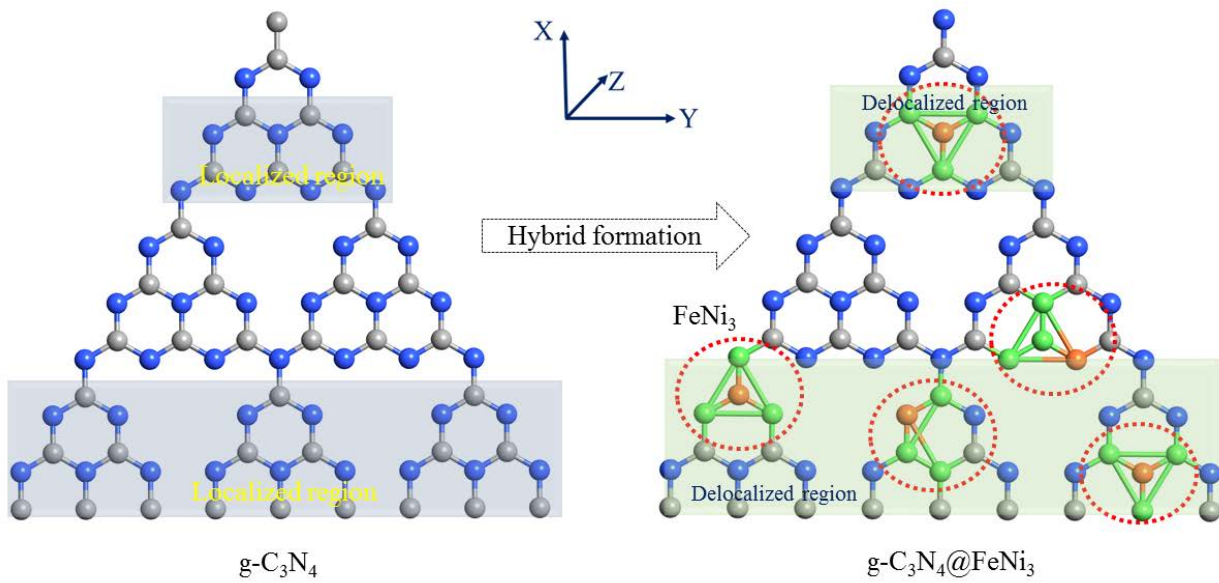


Figure S 10. Stable geometry of the systems in pristine ($\text{g-C}_3\text{N}_4$) and hybrid composite ($\text{g-C}_3\text{N}_4@\text{FeNi}_3$) form. Localized states are shown in pristine form with dark blue transparent cover, which are converted to delocalized states (shown in light green transparent cover) in composite due to metallic nature of the Fe and Ni metal alloy presence. Red dotted circles are used to delocalize FeNi_3 in the hybrid composite.

Absolute atomic Co-ordinates of atoms

Atoms	x	y	z
N	0.5000000000d0	0.2599247842d0	0.5000000000d0
N	0.4069831896d0	0.4261307028d0	0.5000000000d0
N	0.3139663791d0	0.5923366214d0	0.5000000000d0
Ni	0.5930168104d0	0.4261307028d0	0.5000000000d0
N	0.5000000000d0	0.5923366214d0	0.5000000000d0
Ni	0.6860336209d0	0.5923366214d0	0.5000000000d0
N	0.4689943965d0	0.3153267571d0	0.5000000000d0
N	0.3759775860d0	0.4815326757d0	0.5000000000d0
N	0.2829607756d0	0.6477385943d0	0.5000000000d0
N	0.5620112069d0	0.4815326757d0	0.5000000000d0
N	0.4689943965d0	0.6477385943d0	0.5000000000d0
Ni	0.6550280174d0	0.6477385943d0	0.5000000000d0
N	0.4379887930d0	0.3707287300d0	0.5000000000d0
N	0.3449719826d0	0.5369346486d0	0.5000000000d0
N	0.2519551721d0	0.7031405672d0	0.5000000000d0
N	0.5310056035d0	0.5369346486d0	0.5000000000d0
N	0.4379887930d0	0.7031405672d0	0.5000000000d0
N	0.6240224139d0	0.7031405672d0	0.5000000000d0
N	0.4689943966d0	0.4261307028d0	0.5000000000d0
Fe	0.3759775861d0	0.5923366214d0	0.5000000000d0
N	0.5620112070d0	0.5923366214d0	0.5000000000d0
N	0.5310056035d0	0.3153267571d0	0.5000000000d0
N	0.4379887931d0	0.4815326757d0	0.5000000000d0
N	0.3449719826d0	0.6477385943d0	0.5000000000d0
N	0.6240224140d0	0.4815326757d0	0.5000000000d0
Fe	0.5310056035d0	0.6477385943d0	0.5000000000d0
Ni	0.7170392244d0	0.6477385943d0	0.5000000000d0
N	0.5000000000d0	0.3707287300d0	0.5000000000d0
Ni	0.4069831896d0	0.5369346486d0	0.5000000000d0
N	0.3139663791d0	0.7031405672d0	0.5000000000d0
N	0.5930168105d0	0.5369346486d0	0.5000000000d0
Ni	0.5000000000d0	0.7031405672d0	0.5000000000d0
N	0.6860336209d0	0.7031405672d0	0.5000000000d0
Fe	0.5310056035d0	0.4261307028d0	0.5000000000d0
Ni	0.4379887931d0	0.5923366214d0	0.5000000000d0
N	0.6240224140d0	0.5923366214d0	0.5000000000d0
N	0.5620112070d0	0.3707287300d0	0.5000000000d0
N	0.4689943965d0	0.5369346486d0	0.5000000000d0
N	0.3759775861d0	0.7031405672d0	0.5000000000d0
N	0.6550280174d0	0.5369346486d0	0.5000000000d0
N	0.5620112070d0	0.7031405672d0	0.5000000000d0

N	0.7480448279d0	0.7031405672d0	0.5000000000d0
C	0.5000000000d0	0.2968594328d0	0.5000000000d0
C	0.4069831896d0	0.4630653514d0	0.5000000000d0
C	0.3139663791d0	0.6292712700d0	0.5000000000d0
C	0.5930168104d0	0.4630653514d0	0.5000000000d0
Ni	0.5000000000d0	0.6292712700d0	0.5000000000d0
Fe	0.6860336209d0	0.6292712700d0	0.5000000000d0
C	0.4689943965d0	0.3522614057d0	0.5000000000d0
C	0.3759775861d0	0.5184673243d0	0.5000000000d0
C	0.2829607756d0	0.6846732429d0	0.5000000000d0
C	0.5620112070d0	0.5184673243d0	0.5000000000d0
C	0.4689943965d0	0.6846732429d0	0.5000000000d0
C	0.6550280174d0	0.6846732429d0	0.5000000000d0
C	0.4379887930d0	0.4076633786d0	0.5000000000d0
C	0.3449719826d0	0.5738692972d0	0.5000000000d0
C	0.2519551721d0	0.7400752158d0	0.5000000000d0
C	0.5310056035d0	0.5738692972d0	0.5000000000d0
C	0.4379887930d0	0.7400752158d0	0.5000000000d0
C	0.6240224139d0	0.7400752158d0	0.5000000000d0
C	0.5310056035d0	0.3522614057d0	0.5000000000d0
C	0.4379887931d0	0.5184673243d0	0.5000000000d0
C	0.3449719827d0	0.6846732429d0	0.5000000000d0
C	0.6240224140d0	0.5184673243d0	0.5000000000d0
Ni	0.5310056035d0	0.6846732429d0	0.5000000000d0
C	0.7170392244d0	0.6846732429d0	0.5000000000d0
Ni	0.5000000000d0	0.4076633786d0	0.5000000000d0
Ni	0.4069831896d0	0.5738692972d0	0.5000000000d0
C	0.3139663791d0	0.7400752158d0	0.5000000000d0
C	0.5930168105d0	0.5738692972d0	0.5000000000d0
C	0.5000000000d0	0.7400752158d0	0.5000000000d0
C	0.6860336209d0	0.7400752158d0	0.5000000000d0
Ni	0.5620112070d0	0.4076633786d0	0.5000000000d0
C	0.4689943965d0	0.5738692972d0	0.5000000000d0
C	0.3759775861d0	0.7400752158d0	0.5000000000d0
C	0.6550280174d0	0.5738692972d0	0.5000000000d0
C	0.5620112070d0	0.7400752158d0	0.5000000000d0
C	0.7480448279d0	0.7400752158d0	0.5000000000d0

Optimized value of Energy: -1068.094 Ry

Table S2. Positions of atoms of the hybrid nanocomposite formed of g-C₃N₄ and FeNi₃ obtained via geometry optimization. These coordinates fix the minimum energy based stable structure of the composite with a minimum energy of -1068.094 Ry.

Components of Energy		
(Ry)	g-C ₃ N ₄	g-C ₃ N ₄ @FeNi ₃
Kinetic	753.4	977.7
Pseudopotential (local)	-1218.3	-3266.0
Pseudopotential (non-local)	81.9	-279.4
Hartree	572.5	1520.7
Exchange-correlation	-120.9	-321.2
Ewald	431.4	1222.0
Total	-768.83	-1068.094

Table S3. The energy components of the hybrid nanocomposite system gained after geometry optimization to achieve structural stability via BFGS algorithm.

Surface atomic forces and geometry optimization

The forces on atoms at finite radial distance can be calculated from the derivative of the total energy with respect to atomic positions. These calculations lie on the Born-Oppenheimer surface for generalized atomic calculations. This calculation converges to Hellmann-Feynman force by vanishing higher order (i.e. second and third term degree) terms from the master equation. Various energy components of the total energy (Table S2) contains ion-electron terms with both local and non-local pseudopotential contributions. This non-local contribution to the energy and forces are calculated in linear scaling computational effort. As a result, larger systems like hybrid nanocomposite systems can be handled smoothly for *ab initio* DFT calculations.

Gibbs free surface energy profile for energy storage

The Gibbs surface free energy profiles were obtained from the 3×3×1 supercell. The total energy from DFT calculations were obtained as $E^{tot} = [E(Composite) - E(Pristine) - \frac{n}{2}E(G)]$, Thermal corrections were done to calculate adsorption free energy profile. Zero-point energy and temperature dependent entropy contribution are included to find final free energy. The Gibbs free energy of the system was calculated as $E(G) = E^{tot} + 0.22$ eV.

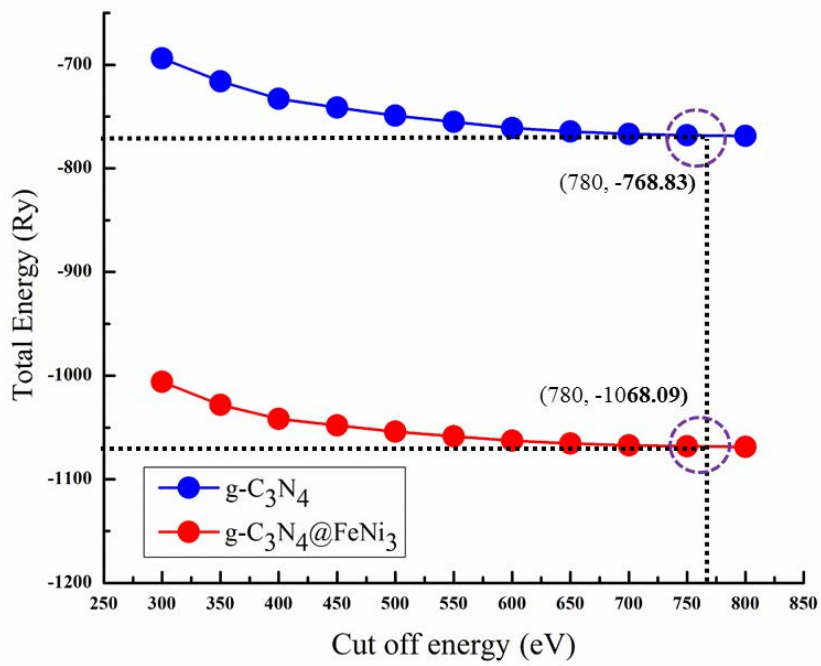


Figure S11. The total energy variation as a function of cut-off energy of the system gained after geometry optimization to achieve structural stability via BFGS algorithm.

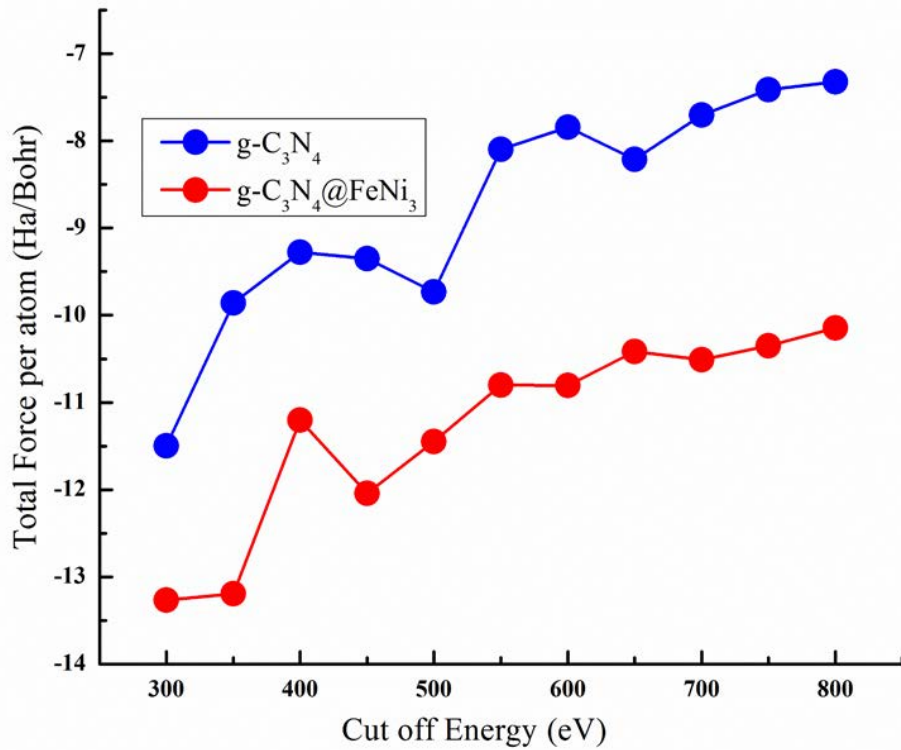


Figure S12. The total force per atom variation as a function of cut-off energy of the system gained after geometry optimization to achieve structural stability via BFGS algorithm.

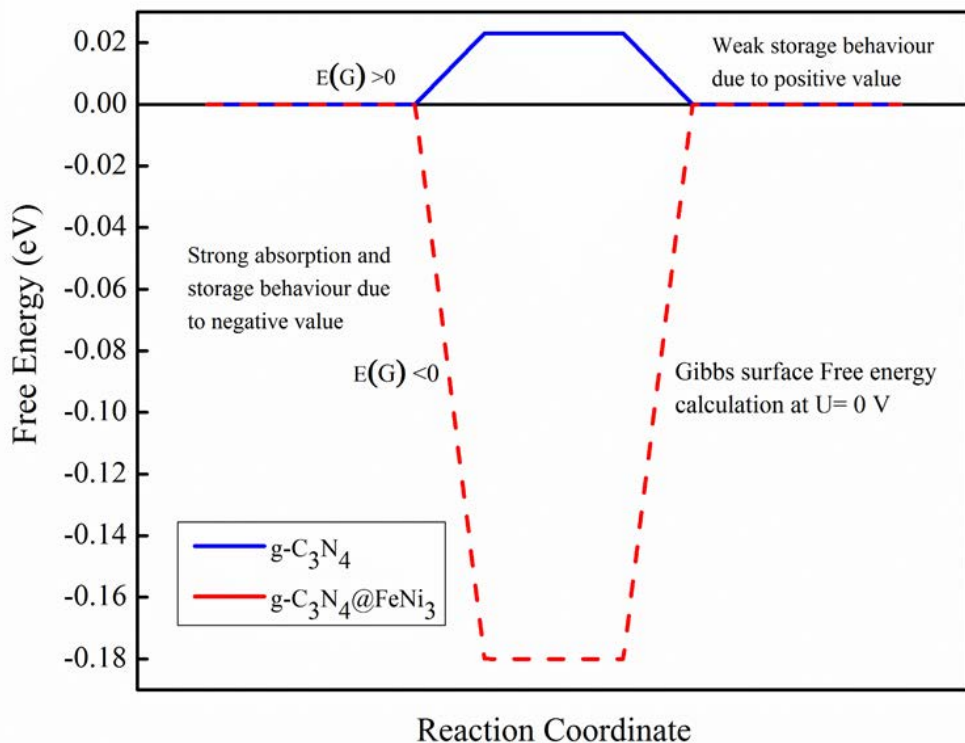


Figure S13. The Free energy value at surface of the systems as a function of reaction coordinates to achieve stability.

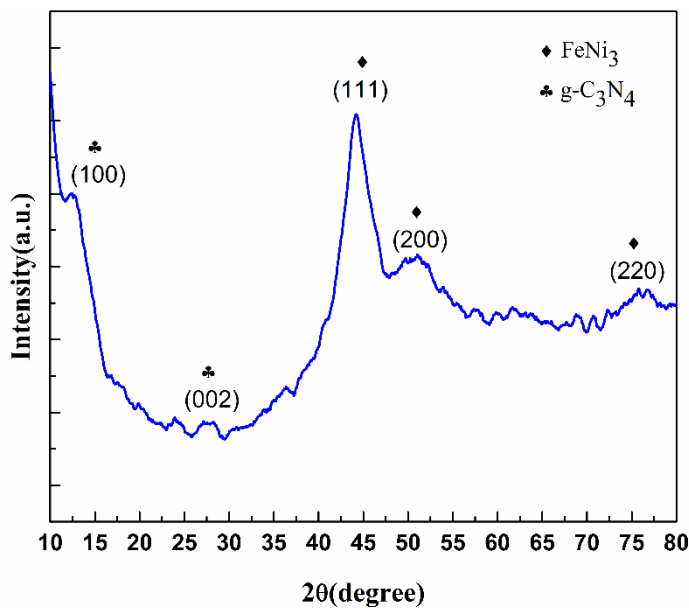


Figure S14. XRD pattern of the heterostructure system.